View metadata, citation and similar papers at core.ac.uk
brought to you by CORE
provided by Purdue E-Pubs

Purdue University
Purdue e-Pubs

Birck and NCN Publications

Birck Nanotechnology Center

5-1-2011

On Electronic Structure Engineering and Thermoelectric Performance

Changwook Jeong
Birck Nanotechnology Center, Purdue University, jeongc@purdue.edu

Mark S. Lundstrom
Birck Nanotechnology Center, Purdue University, lundstro@purdue.edu

Follow this and additional works at: http://docs.lib.purdue.edu/nanopub

Part of the Nanoscience and Nanotechnology Commons

Jeong, Changwook and Lundstrom, Mark S., "On Electronic Structure Engineering and Thermoelectric Performance" (2011). *Birck and NCN Publications.* Paper 1012.
http://docs.lib.purdue.edu/nanopub/1012

This document has been made available through Purdue e-Pubs, a service of the Purdue University Libraries. Please contact epubs@purdue.edu for additional information.

Journal of ELECTRONIC MATERIALS, Vol. 40, No. 5, 2011
DOI: 10.1007/s11664-011-1533-0
© 2011 TMS

On Electronic Structure Engineering and Thermoelectric Performance

CHANGWOOK JEONG[1,2] and MARK LUNDSTROM[1]

1.—Network for Computational Nanotechnology, Birck Nanotechnology Center, Purdue University, West Lafayette, IN, USA. 2.—e-mail: jeongc@purdue.edu

In this paper, we address the question of how to engineer the electronic structure to enhance the performance of a thermoelectric material. We examine several different materials and show that all of them, even those for which giant Seebeck coefficients have been predicted, display a value that is expected from conventional thermoelectric theory. For molecular thermoelectrics, we show that the detailed lineshape plays an important role. Finally, using III–V alloy semiconductors as a model system, we explore the role of electronic structure in the Seebeck coefficient, electrical conductivity, and power factor. In the process, some general guidelines for engineering the electronic component of thermoelectric performance are identified.

Key words: Band-structure engineering, AlGaAs alloy, graphene, molecule, thermoelectric

INTRODUCTION

The dimensionless figure of merit, $ZT = S^2GT/K$, is the primary material parameter governing the maximum thermoelectric (TE) efficiency, where T is temperature, S is the Seebeck coefficient, G is the electrical conductance, and K is the thermal conductance, which is the sum of the electronic contribution, K_e, and the lattice thermal conductance, K_l. For a single, parabolic band material, the Fermi level (E_F) is positioned near the bottom of the conduction band due to the balance between S and G. Most recent improvements in ZT have been achieved by phonon engineering to reduce the lattice thermal conductivity.[1–3] The question of how to improve the electronic performance is now an important one.[4–11]

Significant improvements in S have been predicted and reported for several different materials. For example, an enhanced S has been achieved by engineering the density of states (DOS) in bulk Tl-PbTe[4], the LAST [$(PbTe)_{1-x}(AgSbTe_2)_x$] system,[5] and $La_{3-x}Te_4$,[6] and giant Seebeck coefficients have been predicted for nanostructured graphene[7] and for appropriately engineered molecules.[8] These examples all seek to enhance performance by achieving a delta-function-like DOS. A clear understanding of how electronic structure affects the S and G of a material is essential for developing materials with enhanced power factors (PF) and is the subject of this paper.

In this paper, we:

1. Examine a wide variety of thermoelectric (TE) materials for which large Seebeck coefficients have been predicted.
2. Demonstrate that the Seebeck coefficient for each of them can be explained within the conventional, single-particle framework and show that most materials display similar S versus E_F characteristics.
3. Show for molecular thermoelectrics that the detailed shape of the transmission plays an important role.
4. Use $Al_xGa_{1-x}As$ as a model system to explore the role of electronic structure and significant enhancement in electronic performance is observed due to nonmonotonic behavior of $S(E_F)$.
5. Present general guidelines to enhance the electronic performance of TE devices.

(Received May 14, 2010; accepted January 19, 2011; published online February 19, 2011)

APPROACHES

Our approach, based on the Landauer formalism, is equivalent to the conventional Boltzmann transport equation (BTE) approach,[12] but it adds physical insight and is applicable to quantum-engineered structures as well as to bulk materials.[13,14]

We begin with a brief review of conventional thermoelectric theory and the Landauer formalism. According to conventional thermoelectric theory,[15] integrating the contributions of each energy channel, we find the total S as

$$S = \left(\frac{k_{\rm B}}{q}\right) \int_{-\infty}^{+\infty} \left(\frac{E - E_{\rm F}}{k_{\rm B}T}\right) \frac{G(E)}{G}\, {\rm d}E. \quad (1)$$

This expression can be alternatively expressed as

$$S = -\frac{(E_{\rm C} - E_{\rm F} + \Delta_n)}{qT}, \quad (2)$$

with

$$\Delta_n = \int_{-\infty}^{+\infty} (E - E_{\rm C}) \frac{G(E)}{G}\, {\rm d}E, \quad (3)$$

where Δ_n represents the average energy of charge carriers above the conduction band edge ($E_{\rm C}$). This expression suggests that all materials should display similar S versus $E_{\rm F}$ characteristics within a framework of conventional TE theory and that the band structure should only affect Δ_n. For an ideal single channel, $\Delta_n = 0$, while for nondegenerate materials with parabolic energy bands and constant mean free path (MFP), $\Delta_n = 2k_{\rm B}T$.

To evaluate the Seebeck coefficient, we need to calculate $G(E)$. Within the Landauer formalism, $G(E)$ is given as[14]

$$G(E) = \frac{2q^2}{h} \bar{T}(E) \left(-\frac{\partial f_0}{\partial E}\right), \quad (4)$$

with

$$\bar{T}(E) = T(E)M(E), \quad (5)$$

being the transmission, and $M(E)$ the number of conducting channels. For a conductor of length L, and MFP for backscattering, $\langle\langle \lambda(E) \rangle\rangle$, $T(E)$ is given as

$$T(E) = \langle\langle \lambda(E) \rangle\rangle / L \quad (6)$$

in the diffusive limit. For some common scattering mechanisms, $\langle\langle \lambda(E) \rangle\rangle$ can be expressed in power-law form as $\langle\langle \lambda(E) \rangle\rangle = \lambda_0 (E/k_{\rm B}T)^r$, where λ_0 is a constant, E is the kinetic energy, and r is the characteristic exponent describing a specific scattering process. If we consider a single parabolic conduction band, $E = \hbar^2 k^2 / 2m^*$, then $M(E)$ for three dimensions (3D) is

$$M(E) = A \frac{m^*_{\rm DOM}}{2\pi\hbar^2} (E - E_{\rm C}), \quad (7)$$

where the density-of-modes effective mass, $m^*_{\rm DOM}$, is just m^* for a single, spherical band. For ellipsoidal energy bands, $m^*_{\rm DOM}$ for each equivalent ellipsoid is $\sqrt{m^*_y m^*_z}$ with the direction of current flow being along the x-direction.[14] Procedures for evaluating $M(E)$ from the full band electronic dispersion have been given in Ref. 14.

To explore how the electronic structure can be engineered to enhance performance, three TE devices are examined:

1. Graphene superlattice,[7] for which a 30 mV/K Seebeck coefficient was predicted. $\bar{T}(E)$ is evaluated using the transfer matrix method.
2. A single-molecule device,[8] in which transmission engineering gives rise to a huge increase in S. $\bar{T}(E)$ is taken from the original paper.
3. Ternary materials such as $Al_xGa_{1-x}As$, $Al_xGa_{1-x}Sb$, $Al_xIn_{1-x}As$, and $GaAs_{1-x}P_x$, which are good examples to illustrate the effect of the electronic structure on TE coefficients because
   - the band-splitting, ΔE, and effective masses for Γ, L, and X valleys depend on the Al content.[16]
   - the effective masses of L and X valleys are ~10 times larger than the effective mass of Γ valley.
   - At $x = 0.42$, all valleys are degenerate, and the thermal conductivity is minimum, being 5 and 10 times smaller than the thermal conductivity for GaAs and AlAs, respectively.

RESULTS

Our goal is to discuss, in a single-particle framework, how electronic structure can be engineered to enhance the electronic component of TE performance.

Figure 1a shows the transmission of an infinite graphene sheet and a graphene superlattice (SL).[7] The transmission for graphene is linearly proportional to energy.[17] Since graphene is a zero-gap material, there is a sizable contribution from the valence band. Therefore, the expected maximum S ($S_{\max}$) is only about 100 μV/K. To enhance the Seebeck coefficient, a transmission gap is created by making a periodic graphene p-n junction electrostatically, as shown in Fig. 1a.[7] S is evaluated by the full integral formula (Eq. 1), rather than the simplified Mott formula. Figure 1b compares the S versus $E_{\rm F}$ characteristics of graphene and a graphene SL. It turns out that the predicted 30 mV/K at 300 K is a mathematical artifact caused by inappropriate use of the Mott formula and that the superlattice is no better than graphene.

Significant enhancement in S in single-molecule devices was also predicted by engineering transmission, as shown in Fig. 2a.[8] Figure 2a shows the transmission for a 1,4-biphenyldithiol (BPDT) molecule, for which $S_{\max}$ is found to be ~10 μV/K. This low value is attributed to the relatively flat transmission near the Fermi level, which is in the lowest unoccupied molecular orbital (LUMO)–highest

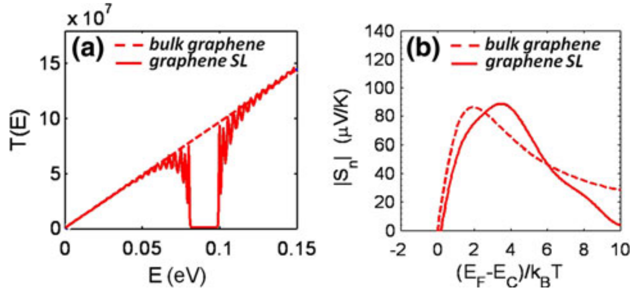

Fig. 1. For graphene and a graphene SL: (a) transmission, and (b) the S versus E_F characteristic.

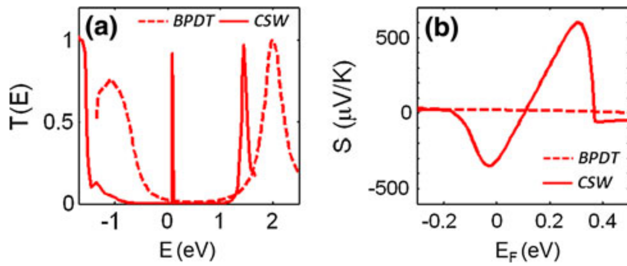

Fig. 2. For a BPDT molecule and a CSW molecule: (a) transmission, and (b) the S versus E_F characteristic.

occupied molecular orbital (HOMO) bandgap region. To enhance S, a very sharp transmission is desirable near the Fermi level. Engineering the transmission is done by putting a side-group on the CSW-470-bipyridine (CSW) molecule, which creates very sharp Fano resonance.[8] In Fig. 2b, the results of BPDT and CSW molecules are compared. Compared with BPDT, CSW shows a huge improvement in S.

DISCUSSION

Questions that will be addressed are:

1. How close are the results for a graphene SL and single molecules to common TE semiconductors? Can all of these be understood within the traditional thermoelectric theory?
2. Why does the Seebeck coefficient for the CSW molecule with the sharp transmission deviate from the single-level model?
3. How can the electronic structure be engineered for maximum TE performance?

The results for graphene, a graphene SL, and a single molecule are compared with common TE semiconductors in Fig. 3. Nanostructured graphene SLs, and an appropriately engineered molecule device display similar $S(E_F)$ characteristics to common semiconductor materials, as expected from Eq. 2. The predicted giant S for a CSW molecule is actually what is expected from a single-level model. For a given Fermi level, the 3D bulk results have a somewhat higher S than the ideal single-level model because, in 3D, energy states are spread out.

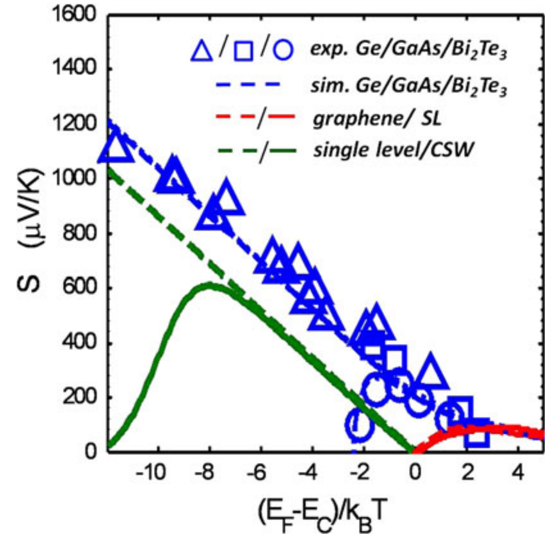

Fig. 3. The results for graphene, a graphene SL, and a single molecule compared with common TE semiconductors.

It is interesting that S for the CSW molecule deviates from a single-level model when E_F is far below the level. The actual Seebeck coefficient is reduced below what we expect from the single-level model by a factor of 30, though the CSW molecule has a very sharp transmission that looks almost like an ideal delta function, as shown in Fig. 2a. This is because the CSW molecule transmission has a finite linewidth with a shape that is actually described by a Lorentzian model where transmission is proportional to E^2. This energy dependency is important because most of the charge and heat flow occurs at the Fermi Level, not at the position of the transmission peak, when E_F is far below the level. In the single-level model, however, all charge and heat should flow at the single channel, no matter where the Fermi level is located. To illustrate the importance of the detailed transmission shape, we compare the results for Gaussian-shaped and Lorentzian-shaped transmissions, as shown in Fig. 4. The results for a Gaussian lineshape, shown by the dashed line, follow exactly the single-level model, albeit with large standard deviation. The Seebeck coefficient for a Lorentzian lineshape, however, shows degradation from the single-level model, and the maximum Seebeck coefficient depends on the value of the standard deviation.

Since all materials examined so far display similar Seebeck coefficient behavior, it is essential to consider other approaches for enhancing S by electronic structure engineering. Using ideas similar to those of Ref. 4, it will be shown that enhancing the electronic component of TE performance is possible even in common semiconductors such as $Al_xGa_{1-x}As$, just by changing the Al content.

For varying content of Al, relevant parameters are taken from Ref. 16, and linear interpolation is used for unknown parameters. Although the

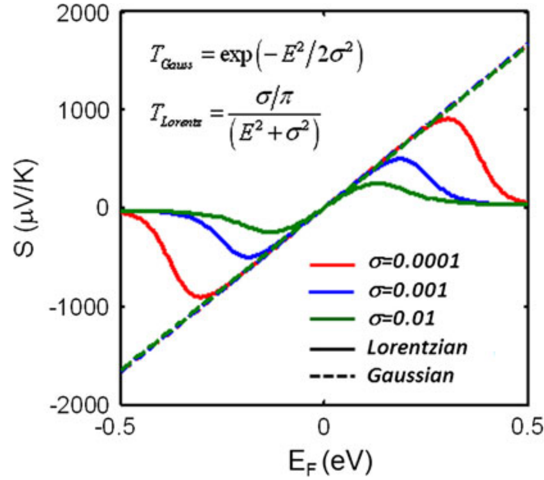

Fig. 4. Comparison of the results for Gaussian-shaped and Lorentzian-shaped transmission with respect to the standard deviation (σ).

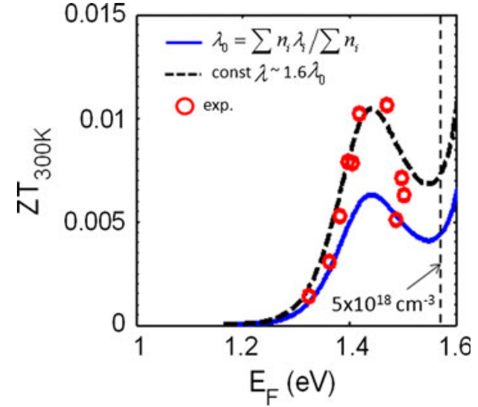

Fig. 5. Calculation of ZT for GaAs ($x = 0$ in $Al_xGa_{1-x}As$) with the best-fit λ_0 and Eq. 9, compared with experimental results.[24]

scattering parameters generally depend on the location of the Fermi level, the average MFP, $\langle\langle\lambda(E)\rangle\rangle$, is assumed to be energy independent, λ_0, because calculations with the constant λ_0 approximation[14] turned out to be in good agreement with experiments over a wide range of doping densities (or E_F level) for common semiconductors. (Others have found similarly good agreement with experimental data by solving the BTE in the constant relaxation time approximation.[18,19]) As shown in Fig. 5, calculations with a constant mean free path (black dashed line) match well with experiments over the range of E_F of interest, also capturing well the maximum value of the PF. The constant λ_0 is estimated as follows. Firstly, λ_i for each valley i is calculated using the 3D expression for MFP for backscattering.[14]

$$\lambda_i = \frac{4}{3}\upsilon_T\tau_i = \frac{4}{3}\sqrt{\frac{2m_c^* k_B T}{\pi q^2}}\mu_i, \tag{8}$$

with μ_i and m_c^* being the experimentally determined mobility and the conductivity effective mass, respectively.[20] The overall λ_0 is estimated by weighting λ_i in each valley by the electron population density of the ith valley, n_i.[21]

$$\lambda_0 = \sum_{i\ \text{valley}} n_i\lambda_i \Big/ \sum_{i\ \text{valley}} n_i. \tag{9}$$

Figure 5 compares the calculation of ZT for GaAs ($x = 0$ in $Al_xGa_{1-x}As$) with the best-fit λ_0 and Eq. 9. Although Eq. 9 underestimates the experimental results by about 50%, this does not affect the comparison of $Al_xGa_{1-x}As$ alloy with pure GaAs and AlAs. The comparisons are the subject of this study. It is also assumed that the upper limit of the doping density is 5×10^{18} cm^{-3}.

For each Al content, the optimum position of the Fermi level (doping density) is determined for maximum ZT. The resulting optimum TE parameters (S, G, K, PF, ZT) are shown in Fig. 6. Comparing with GaAs ($x = 0$), a 5 times enhancement in PF and 10 times enhancement in ZT are predicted at $x = 0.28$ and 0.29, respectively. Interestingly, maximum ZT is not achieved at an Al concentration of 0.42 where all valleys are degenerate and the thermal conductivity is minimum. When $x \geq 0.06$, the optimum doping density for maximum ZT is the maximum allowed doping of 5×10^{18} cm^{-3}, which causes $S(G)$ suddenly to decrease (increase) at $x = 0.06$. The reason why $S(G)$ gradually increases (decreases) at $x \geq 0.06$ is that nonmonotonic behavior of S versus E_F is noticeable, as shown in Fig. 7b and c.

Figure 7 shows S, G, and PF versus Fermi level for Al contents of 0, 0.17, 0.28, and 0.42. For pure GaAs ($x = 0$), a conventional monotonic $S(E_F)$ is observed up to $E_F = 5k_BT$, at which the Seebeck coefficient starts increasing again with E_F due to the L valley contribution. Also the optimum doping density is below the maximum allowed doping of 5×10^{18} cm^{-3}. At $x = 0.17$ and $x = 0.28$, the nonmonotonic $S(E_F)$ characteristic becomes prominent, giving rise to high S and PF at the degenerate limit, whereas the totally degenerate condition ($x = 0.42$) does not show enhancement in PF, mainly due to low mobility. This nonmonotonic S was also reported in bulk Tl-PbTe[4]. Note that the upper limit of doping density, shown by the dashed line, is the optimum doping density for maximum PF at $x = 0.17$, $x = 0.28$, and $x = 0.42$.

The DOS at $x = 0.17$ and $x = 0.28$ are shown in Fig. 8. The band-splitting (ΔE) between Γ and L is 5 to 7 times k_BT, and the effective density-of-states mass (m^*_{DOS}) and density-of-modes mass (m^*_{DOM}) for the L valley are 7 and 20 times larger than for the Γ valley, respectively. The L valley with heavy effective mass is analogous to the resonant states in bulk Tl-PbTe[4]. To find a general guideline for the effective mass ratio (m_2^*/m_1^*) between the lower (m_1^*)

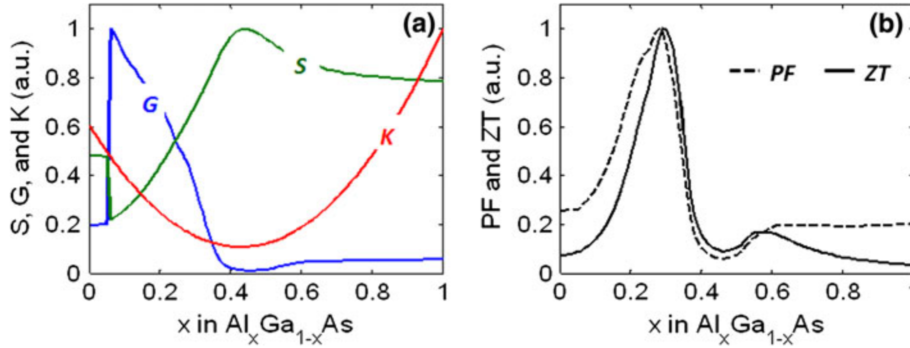

Fig. 6. (a) Optimum S, G, and K, and (b) PF and ZT with respect to Al content.

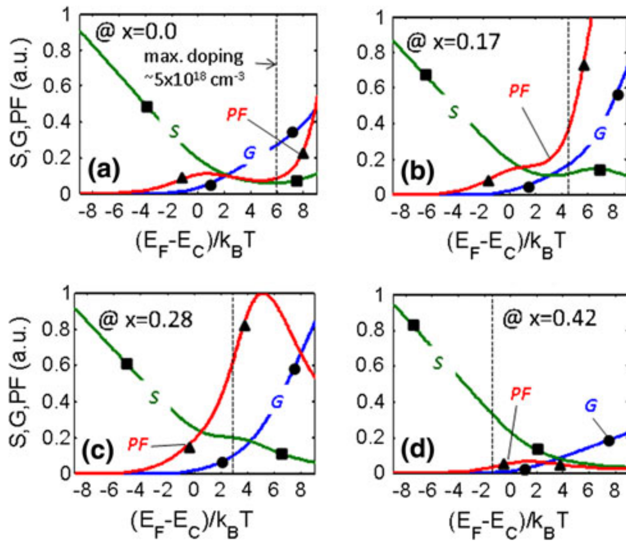

Fig. 7. S, G, and PF versus Fermi level for Al content of (a) 0, (b) 0.17, (c) 0.28, and (d) 0.42.

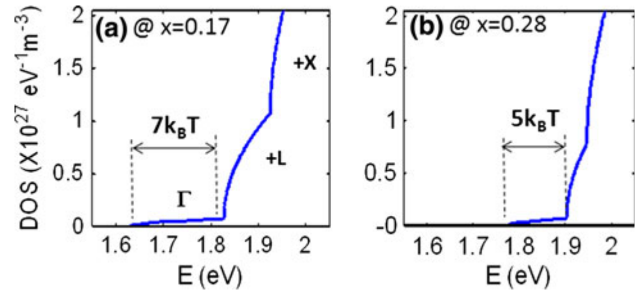

Fig. 8. Density of states at (a) x = 0.17 and (b) x = 0.28.

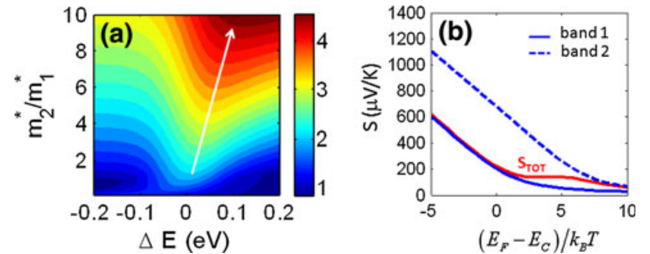

Fig. 9. (a) Calculation of maximum PF for the simple two-band model, normalized by the maximum PF obtained for the one-band case. (b) S versus E_F characteristics at the maximum PF condition.

and upper valley (m_2^*) and band-splitting (ΔE) to achieve maximum PF, two simple parabolic bands case are studied. Unlike $Al_xGa_{1-x}As$, in this simple model, the effective mass ratio and band-splitting (ΔE) can be varied without constraint.

Calculation of the maximum PF for the simple two-band model is shown in Fig. 9a, where the results are normalized by the maximum PF obtained for the one-band case. Similar to the case of $Al_xGa_{1-x}As$ with x = 0.28, an increase in PF of about 5 times is achieved when $m_2^*/m_1^* = 10$ and $\Delta E \approx 5k_BT$. As shown in Fig. 9b, a nonmonotonic S versus E_F behavior is also observed at the maximum PF condition.

Figure 10 shows under which condition nonmonotonic S occurs. The band splitting between the two bands is kept at $5k_BT$, and we examine the effects of effective mass of the upper band on the S versus E_F characteristics. Nonmonotonic behavior of S starts appearing when the effective mass ratio is larger than 5 as shown in Fig. 10a. In Fig. 10b, the band splitting varies, with m_2^*/m_1^* kept at 10. In the case where the band splitting is above $4k_BT$, nonmonotonic behavior of S is observed. When the two bands are very close, their S follows conventional thermoelectric theory.

Generally, the higher m_2^*/m_1^* is, the better the PF, because higher m_2^*/m_1^* is desirable for nonmonotonic $S(E_F)$. For maximum PF, a certain amount of band splitting (ΔE) is needed for both nonmonotonic $S(E_F)$ and suppression of scattering, which is due to the fact that our model assumes that the scattering rates increase with the DOS. This is the case for phonon-dominated scattering and scattering from a delta-function-like perturbing potential such as for defects.[22] Considering a typical doping limit,[23] the optimum band-splitting might be on the order of $5k_BT$.

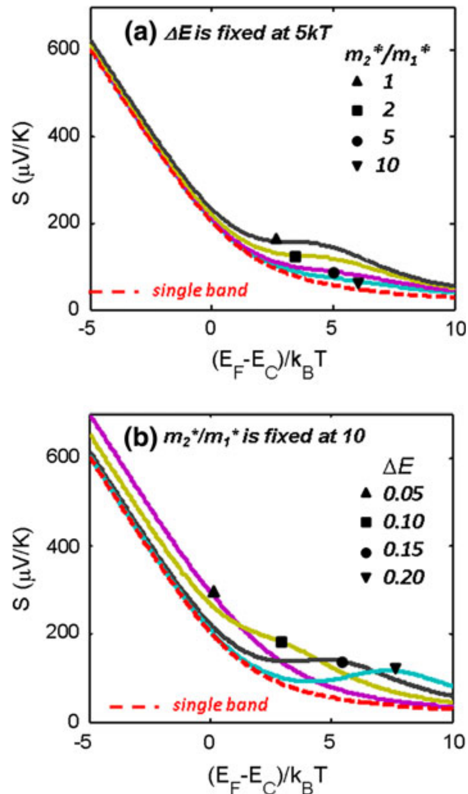

Fig. 10. S versus E_F characteristics: (a) with the band splitting kept at $5k_BT$, and (b) with m_2^*/m_1^* kept at 10. The band splitting, ΔE, is in the units of eV.

CONCLUSIONS

It is shown herein that most materials display a similar monotonic behavior of S versus E_F, but for molecular thermoelectrics, the detailed lineshape of the transmission plays an important role. In the $Al_xGa_{1-x}As$ material system, an increase in PF of 5 times and in ZT of 10 times is possible because of the nonmonotonic S behavior, which maintains high S at high carrier densities, resulting in high PF. This result is similar to the behavior reported for bulk Tl-PbTe[4]. This increase only happens when multiple bands are engineered in an appropriate way. General guidelines for electronic structure engineering are as follows: (1) an upper band with a heavy m^* (equivalently, sharp resonant states) is needed, and (2) the minimum of the upper band must be about $5k_BT$ above the lower, dispersive band. The appropriate band structure may be achieved with an alloy of the proper composition (as discussed herein), by the introduction of resonant states (as discussed in Ref. 4) or by proper strain engineering.

ACKNOWLEDGEMENTS

This work was supported by the National Science Foundation under Grant ECS-0609282 and by the Semiconductor Research Corporation Focus Center in Material, Structure, and Devices. C.J. would like to thank R. Kim and S. Salamat for fruitful discussions.

REFERENCES

1. A. Majumdar, *Science* 303, 777 (2004).
2. G.J. Snyder and E.S. Toberer, *Nat. Mater.* 7, 105 (2008).
3. G. Chen, M.S. Dresselhaus, G. Dresselhaus, J.P. Fleurial, and T. Caillat, *Int. Mater. Rev.* 48, 45 (2003).
4. J.P. Heremans, V. Jovovic, E.S. Toberer, A. Saramat, K. Kurosaki, A. Charoenphakdee, S. Yamanaka, and G.J. Snyder, *Science* 321, 554 (2008).
5. D. Bilc, S.D. Mahanti, E. Quarez, K.-F. Hsu, R. Pcionek, and M.G. Kanatzidis, *Phys. Rev. Lett.* 93, 146403 (2004).
6. A.F. May, D.J. Singh, and G.J. Snyder, *Phys. Rev. B* 79, 153101 (2009).
7. D. Dragoman and M. Dragoman, *Appl. Phys. Lett.* 91, 203116-3 (2007).
8. C.M. Finch, V.M. Garcia-Suarez, and C.J. Lambert, *Phys. Rev. B* 79, 033405-4 (2009).
9. T. Koga, X. Sun, S.B. Cronin, and M.S. Dresselhaus, *Appl. Phys. Lett.* 73, 2950 (1998).
10. T. Thonhauser, T.J. Scheidemantel, J.O. Sofo, J.V. Badding, and G.D. Mahan, *Phys. Rev. B* 68, 85201 (2003).
11. A. Bentien, S. Johnsen, G.K.H. Madsen, B.B. Iversen, and F. Steglich, *Europhys. Lett.* 80, 17008 (2007).
12. G.D. Mahan and J.O. Sofo, *Proc. Natl. Acad. Sci.* 93, 7436 (1996).
13. M. Lundstrom, *ECE 656 Lecture 17: BTE and Landauer* (http://nanohub.org/resources/7509, 2009).
14. C. Jeong, R. Kim, M. Luisier, S. Datta, and M. Lundstrom, *J. Appl. Phys.* 107, 023707 (2010).
15. H. Fritzsche, *Solid State Commun.* 9, 1813 (1971).
16. S. Adachi, *Properties of Aluminum Gallium Arsenide* (The Institution of Engineering and Technology, 1993).
17. M. Lundstrom, *ECE 656 Lecture 4: Density of States—Density of Modes* (http://nanohub.org/resources/7349, 2009).
18. T.J. Scheidemantel, C. Ambrosch-Draxl, T. Thonhauser, J.V. Badding, and J.O. Sofo, *Phys. Rev. B* 68, 125210 (2003).
19. S. Lee and P. Allmen, *Appl. Phys. Lett.* 88, 022107-3 (2006).
20. A.K. Saxena and K.S. Gurumurthy, *J. Phys. Chem. Solids* 43, 801 (1982).
21. M.W. Cresswell and J.P. McKelvey, *Phys. Rev.* 144, 605 (1966).
22. M. Lundstrom, *Fundamentals of Carrier Transport*, 2nd ed. (Cambridge: Cambridge University Press, 2000).
23. R.C. Newman, *Mater. Sci. Eng. B Solid* 66, 39 (1999).
24. G. Homm, P.J. Klar, J. Teubert, and W. Heimbrodt, *Appl. Phys. Lett.* 93, 042107-3 (2008).

Copyright of Journal of Electronic Materials is the property of Springer Science & Business Media B.V. and its content may not be copied or emailed to multiple sites or posted to a listserv without the copyright holder's express written permission. However, users may print, download, or email articles for individual use.